ELSEVIER

Mechanics of Materials 18 (1994) 89–101

MECHANICS OF MATERIALS

Fractal nature of material microstructure and size effects on apparent mechanical properties

Alberto Carpinteri

Politecnico di Torino, Department of Structural Engineering, 10129 Torino, Italy

Received 2 November 1992; revised version received 24 May 1993

Abstract

The problems of the size effects on tensile strength and fracture energy of brittle and disordered materials (concrete, rocks, ceramics, etc.) are reconsidered under a new and unifying light cast on by fractal geometry. It is physically impossible to measure constant material properties, unless we depart from integer dimensions of the material ligament at peak stress and of the fracture surface at final rupture. In this way we can define new tensile properties with physical dimensions depending on the fractal dimension of the damaged microstructure, which turn out to be scale-invariant material constants. This represents the so-called renormalization procedure, already proposed in the statistical physics of random processes. Variations in the fractal dimension of fracture surfaces produce variations in the physical dimension of toughness, and not, as asserted by some authors, only in the measure of toughness. In disordered materials an attenuation of the size effects due to the dimensional disparity between strength and toughness is found. As a limit case, any size effect vanishes when both tensile strength and fracture energy present the physical dimension characteristic of the stress-intensity factor, $[F]\,[L]^{-3/2}$. It is very likely that this critical situation is achieved only inside a very disorderly damaged microstructure, e.g., in the vicinity of the crack tip. In the case of tensile strength, the dimensional decrement represents self-similar weakening of the material ligament, due to pores, voids, defects, cracks, aggregates, inclusions, etc. Analogously, in the case of fracture energy, the dimensional increment represents self-similar tortuosity of the fracture surface, as well as self-similar overlapping and distribution of microcracks in the direction orthogonal to that of the forming macrocrack.

1. Introduction

Size-scale effects on tensile strength and fracture toughness have been recurrent subjects of research as well as relevant topics in the scientific literature of the last few years (Carpinteri, 1986a; Mazars et al., 1989). In spite of the many explanations given to the single specific trends (Carpinteri and Ingraffea, 1984; Shah and Carpinteri, 1991; Carpinteri, 1992; van Mier et al., 1991; Hu and Wittmann, 1992; Guinea et al., 1992; Planas et al., 1992; Elices et al., 1992), no unitary explanation based on very general concepts has so far been put forward. In this paper a new theoretical interpretation will be proposed according to the actual fractal nature of the reference spaces used in classical solid mechanics. A fractal space is a mathematical domain with a non-integer dimension. This is an old concept, recently reintroduced and systematized by Mandelbrot (1982), Falconer (1990) and other authors, which presents a wide field of applications

0167-6636/94/$07.00
SSDI 0167-6636(94)00008-5

in modern technology. For example, the weight of several spongy objects does not increase proportionally to the volume, because they present a non-constant classical density, understood as mass over volume, although it is possible to define a constant "universal" density, understood as mass over length raised to the fractal dimension of the space occupied by the object. This dimension is comprised between 2 and 3.

The fractal view of solid mechanics could be considered as one of the most important examples of transcending the bounds of classical continuum mechanics (Panagiotopoulos, 1992). In the present century we have had more than one such conceptual revolution, according to Popper. Quantum Mechanics and Catastrophe Theory could be mentioned among the most general, even if Griffith's (1921) and Irwin's (1957) ideas are not overlooked in the field of strength of materials, where surface energy and, especially, the stress-intensity factor are non-conventional quantities having unusual physical dimensions.

The *middle-third Cantor set*, which is a typical fractal set, may be constructed from a unit interval by a sequence of deletion operations (Fig. 1). Let E_0 be the interval [0,1]. Let E_1 be the set obtained by deleting the middle third of E_0, so that E_1 consists of the two intervals $[0, \frac{1}{3}]$ and $[\frac{2}{3}, 1]$. Deleting the middle thirds of these intervals gives E_2; thus E_2 comprises the four intervals $[0, \frac{1}{9}]$, $[\frac{2}{9}, \frac{1}{3}]$, $[\frac{2}{3}, \frac{7}{9}]$, $[\frac{8}{9}, 1]$. Proceeding in like manner, E_k is obtained by deleting the middle third of each interval in E_{k-1}. Thus E_k consists of 2^k intervals each of length 3^{-k}. The middle-third Cantor set is the intersection $\bigcap_{k=0}^{\infty} E_k$, and thus may be thought of as the limit of the sequence of sets E_k as k tends to infinity. The length of the middle-third Cantor set is zero as the limit $(2/3)^k \to 0$ for $k \to \infty$. It will be demonstrated, however, that the fractal dimension of the set is 0.631, and therefore that it can be measured consistently only as a length raised to 0.631.

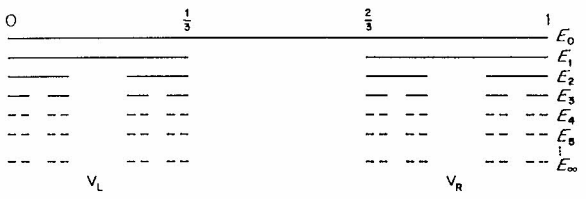

Fig. 1. Middle-third Cantor set (fractal dimension = 0.631).

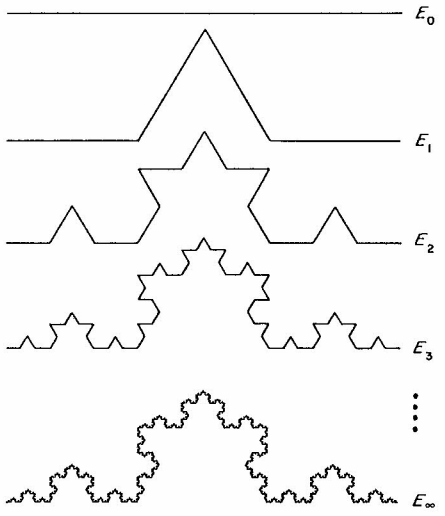

Fig. 2. Von Koch curve (fractal dimension = 1.262).

A second example of a fractal set, with dimension larger than one, is the *von Koch curve* (Fig. 2). Let E_0 be a line segment of unit length. The subset E_1 consists of the four segments obtained by removing the middle third of E_0 and replacing it by the other two sides of the equilateral triangle based on the removed segment. We construct E_k by applying the same procedure to each of the segments in E_{k-1}, and so on. The sequence of polygonal curves E_k approaches the von Koch curve as k tends to infinity. The length of the von Koch curve tends to infinity as $(4/3)^k$ does for $k \to \infty$. The fractal dimension of the curve is 1.262, the dimensionality increase of 0.262 being due to its tortuosity. The curve could then be measured only as a length raised to 1.262.

The systematic error that has been repeated in measuring strength and toughness of disordered materials, such as concrete and rocks, is that of considering reference areas and volumes with the ideal integer dimensions of 2 and 3, respectively. If this error is made in the scale range over which the fractal properties hold, it will be physically impossible to measure constant material properties, unless we abandon integer dimensions of the

material ligament at peak stress and of the fracture surface after stress relaxation or at final rupture. Defining new tensile properties with physical dimensions depending on the fractal dimension of the damaged material microstructure, represents the so-called renormalization procedure, already utilized in the statistical physics of random processes (Herrmann and Roux, 1990). In this way it is possible to obtain the so-called "universal" properties, i.e. scale-invariant material constants.

Some authors have recently endeavoured to link the fractal dimension of the fracture surface to fracture toughness K_{IC} (Mackin et al., 1990; Long et al., 1991). This attempt has not been successful, in particular because the physical dimension of K_{IC} was not assumed to vary with the fractal dimension of the surface. A variation in the physical dimension of fracture toughness (and hence of fracture energy), together with an analogous variation of tensile strength, turns out to provide an attenuation of the scale effects due to the dimensional disparity between strength and toughness. For a very disordered material the attenuation is complete and any scale effect vanishes, both tensile strength and fracture energy being [force] $\times$ [length]$^{-1.5}$. Similar attenuations were emphasized and analyzed by the writer for strain-hardening materials in the presence of cracks (Carpinteri, 1983) and for linear elastic materials in the presence of re-entrant corners (Carpinteri, 1987).

2. Hausdorff dimension

If U is a subset of the n-dimensional Euclidean space, R^n, the *diameter* of U is defined as the greatest distance apart of any pair of points in U:

$$|U| = \sup\{|x-y|: x, y \in U\}. \tag{1}$$

We say that a countable (or finite) collection of sets of diameter at most δ that covers V:

$$\bigcup_{i=1}^{\infty} U_i \supset V, \tag{2}$$

with $0 < |U_i| \leqslant \delta$, $\forall i$, is a *δ-cover* of V.

Suppose that V is a subset of R^n and α is a non-negative number. For any $\delta > 0$ we define:

$$\mathscr{M}_{\delta}^{\alpha}(V) = \inf\left\{ \sum_{i=1}^{\infty} |U_i|^{\alpha}: \{U_i\} \text{ is a } \delta\text{-cover of } V \right\}, \tag{3}$$

and then the *α-dimensional Hausdorff measure* of V is given by the limit:

$$\mathscr{M}^{\alpha}(V) = \lim_{\delta \to 0} \mathscr{M}_{\delta}^{\alpha}(V). \tag{4}$$

The Hausdorff measure is always 0 or ∞, except for one particular value of $\alpha = \bar{\alpha}$, which is called the *Hausdorff dimension* of the set V. The Hausdorff dimension generalizes the familiar concepts of length, area and volume: $\mathscr{M}^0(V)$ is the number of points of a discrete set V; $\mathscr{M}^1(V)$ gives the length of a smooth curve V; $\mathscr{M}^2(V)$ gives the area of a smooth surface; $\mathscr{M}^3(V)$ gives the volume of a "non-spongy" 3-dimensional domain V.

The scaling properties of length, area and volume are well-known. On magnification by a factor λ, the length of a curve is multiplied by λ, the area of a surface is multiplied by λ^2 and the volume of a 3-dimensional domain is multiplied by λ^3. On the other hand, the α-dimensional Hausdorff measure scales with a factor λ^{α}:

$$\mathscr{M}^{\alpha}(\lambda V) = \lambda^{\alpha} \mathscr{M}^{\alpha}(V), \tag{5}$$

where $\lambda V = \{\lambda x: x \in V\}$ is the set V scaled by a factor λ.

A graph of $\mathscr{M}^{\alpha}(V)$ against α (Fig. 3) shows that there is a critical value of $\alpha = \bar{\alpha}$ at which

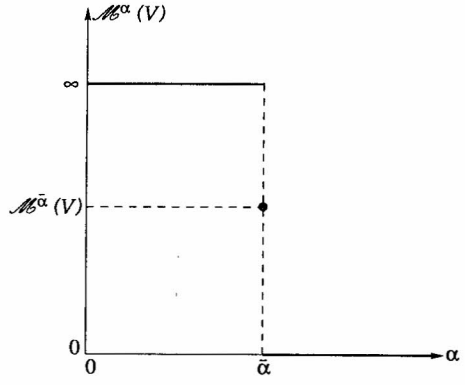

Fig. 3. α-dimensional Hausdorff measure of a set against the parameter α.

$\mathcal{M}^\alpha(V)$ jumps from ∞ to 0. This critical value is called the *Hausdorff dimension* of V:

$$\bar{\alpha} = \dim_H V = \inf\{\alpha: \mathcal{M}^\alpha(V) = 0\} = \sup\{\alpha: \mathcal{M}^\alpha(V) = \infty\}. \quad (6)$$

If $\alpha = \bar{\alpha} = \dim_H V$, then $\mathcal{M}^\alpha(V)$ is finite if V is finite. For example, a flat disc of unit radius presents infinite length and null volume, and, more generally, $\mathcal{M}^\alpha(V) = \infty$ if $\alpha < 2$ and $\mathcal{M}^\alpha(V) = 0$ if $\alpha > 2$, whereas $\mathcal{M}^2(V) = \pi$.

Reconsider the *middle-third Cantor set* (Fig. 1). A heuristic calculation of the Hausdorff dimension may be developed by observing that the Cantor set splits into a left part $V_L = V \cap [0, \frac{1}{3}]$ and a right part $V_R = V \cap [\frac{2}{3}, 1]$. Both parts are geometrically similar to V but scaled by a ratio $\frac{1}{3}$, and $V = V_L \cup V_R$ with this union disjoint. Thus for any α:

$$\mathcal{M}^\alpha(V) = \mathcal{M}^\alpha(V_L) + \mathcal{M}^\alpha(V_R) = \left(\tfrac{1}{3}\right)^\alpha \mathcal{M}^\alpha(V) + \left(\tfrac{1}{3}\right)^\alpha \mathcal{M}^\alpha(V), \quad (7)$$

according to Eq. (5). If we divide both sides of Eq. (7) by the Hausdorff measure $\mathcal{M}^\alpha(V)$, assumed as being a finite quantity, we obtain:

$$1 = 2\left(\tfrac{1}{3}\right)^\alpha, \quad \text{or} \quad \alpha = \ln 2/\ln 3. \quad (8)$$

For the *von Koch curve* (Fig. 2) an analogous balance may be written:

$$1 = 4\left(\tfrac{1}{3}\right)^\alpha, \quad \text{or} \quad \alpha = \ln 4/\ln 3. \quad (9)$$

The preceding heuristic method gives the right answer for the dimension of several fractal sets. More generally, if $V = \bigcup_{i=1}^m V_i$, where each V_i is geometrically similar to V but scaled by a different factor c_i, then the heuristic argument gives $\dim_H V$ as the root α of the equation:

$$\sum_{i=1}^m c_i^\alpha = 1. \quad (10)$$

Consider the *uniform Cantor set* of Fig. 4, with $m = 3$ and $\lambda = \frac{4}{15}$. In this case the balance is:

$$1 = 3\left(\tfrac{4}{15}\right)^\alpha,$$

or

$$\alpha = \ln \tfrac{1}{3}/\ln \tfrac{4}{15} \simeq 0.831. \quad (11)$$

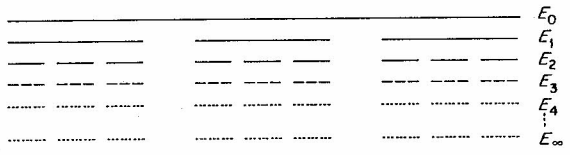

Fig. 4. Uniform Cantor set (fractal dimension = 0.831).

More generally, for an integer $m \geq 2$ and $0 < \lambda < 1/m$, it is possible to prove that:

$$\dim_H V = -\ln m/\ln \lambda, \quad (12a)$$

$$0 < \mathcal{M}^{-\ln m/\ln \lambda}(V) < \infty. \quad (12b)$$

The case of the *modified von Koch curve* (Fig. 5) involves for instance more than one ratio in Eq. (10). If we fix $0 < a < \frac{1}{3}$ and construct a curve V by repeatedly replacing the middle proportion a of each interval by the other two sides of an equilateral triangle, then $\dim_H V$ is the solution of the equation:

$$1 = 2a^\alpha + 2\left[\tfrac{1}{2}(1-a)\right]^\alpha. \quad (13)$$

Observe that the Hausdorff dimension of the related uniform Cantor set, with $m = 2$ and $\lambda = \frac{1}{2}(1-a)$, is given by:

$$1 = 2\left[\tfrac{1}{2}(1-a)\right]^\alpha. \quad (14)$$

An application of Eq. (10) provides the Hausdorff dimension of the fractal curve in Fig. 6. The lengths of the segments in the *generator* are respectively $\frac{1}{3}$, $\frac{1}{4}$, $\frac{1}{3}$, $\frac{1}{4}$, $\frac{1}{3}$, and the balance is:

$$1 = 3\left(\tfrac{1}{3}\right)^\alpha + 2\left(\tfrac{1}{4}\right)^\alpha,$$

or

$$\alpha \simeq 1.34. \quad (15)$$

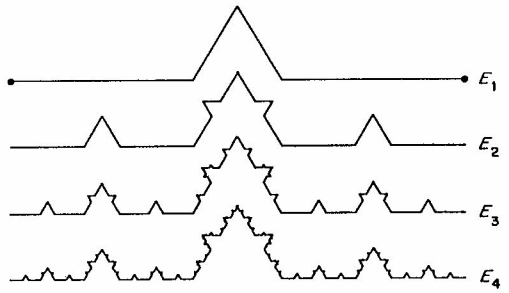

Fig. 5. Modified von Koch curve.

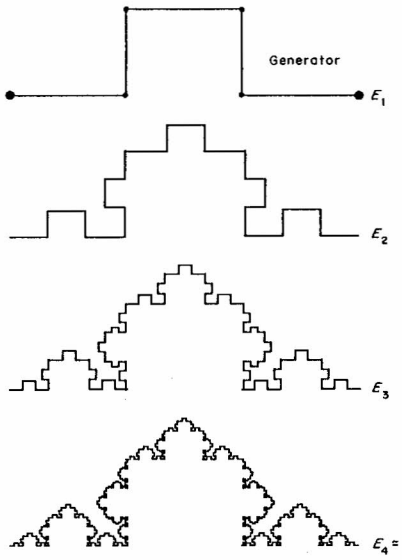

Fig. 6. Fractal curve (fractal dimension = 1.34).

Whereas the von Koch curve is an example of dimensionality increment due to tortuosity and meandering at different scales, we may obtain a similar increment even from overlapping at different scales. Let us consider the interval $[0, 1] = [0, \frac{2}{3}] \cup [\frac{1}{3}, 1]$ and then, recursively, $[0, \frac{2}{3}] = [0, \frac{4}{9}] \cup [\frac{2}{9}, \frac{2}{3}]$, $[\frac{1}{3}, 1] = [\frac{1}{3}, \frac{7}{9}] \cup [\frac{5}{9}, 1]$, etc. (Fig. 7). The balance equation is therefore:

$$1 = 2\left(\tfrac{2}{3}\right)^{\alpha}, \tag{16}$$

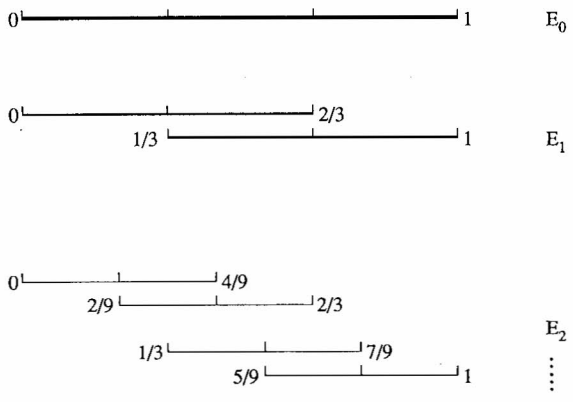

Fig. 7. Fractal set obtained from overlapping at different scales (fractal dimension = 1.709).

or

$$\alpha = \frac{\ln 2}{\ln 3 - \ln 2} \simeq 1.709. \tag{17}$$

3. Box-counting dimension

The Hausdorff dimension, discussed in the previous section, is the principal definition of dimension for fractal geometries. On the other hand, other definitions can be proposed from a practical point of view. Fundamental to most definitions of dimension is the idea of "measurement at scale δ". For each δ, we measure a set in a way that ignores irregularities of a size less than δ, and we see how these measurements behave as $\delta \to 0$. For example, if V is a plane curve (e.g. a coastline or the course of a river), the measurement $M_\delta(V)$ might be represented by the number of discrete and rectilinear steps of length δ necessary to approximate V with a polygonal curve. The dimension of V is then determined by the power law obeyed by $M_\delta(V)$ as $\delta \to 0$:

$$M_\delta(V) = c\delta^{-\alpha}, \tag{18}$$

where α is the so-called *box-counting dimension* and c is the length of the polygonal curve for $\delta = 1$. In the case of an ideal regular curve, it is well-known from classical geometry that $\alpha = 1$. Taking logarithms:

$$\ln M_\delta(V) = \ln c - \alpha \ln \delta. \tag{19}$$

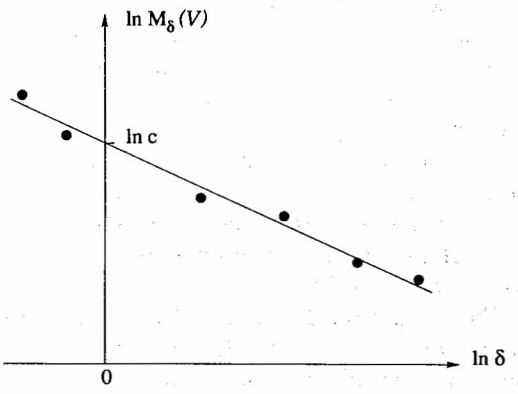

Fig. 8. Definition of box-counting dimension.

This formula is useful for experimental purposes, since α can be estimated as the gradient of a bi-logarithmic graph plotted over a suitable range of δ (Fig. 8). Usually this range is limited. For example, for concrete the lower and upper bounds could be in some connection with the extremities in the granulometric curve.

To find the box dimension of a plane set V we may draw a mesh of squares or boxes of side δ and count the number $M_\delta(V)$ that overlap the set for various small δ. The dimension is the logarithmic rate at which $M_\delta(V)$ increases as $\delta \to 0$. The number of mesh squares or cubes of side δ that intersect a set is an indication of how spread-out or irregular the set is when examined at scale δ. The dimension reflects how rapidly the irregularities develop as $\delta \to 0$.

For the middle-third Cantor set, the covering E_k gives (Fig. 1):

$$\delta = 3^{-k}, \tag{20a}$$

$$M_\delta(V) = 2^k, \tag{20b}$$

and then, from Eq. (19):

$$k \ln 2 = \ln 1 + k\alpha \ln 3, \tag{21}$$

or $\alpha = \ln 2/\ln 3$.

For the von Koch curve an analogous reasoning holds.

4. Random fractals

Many of the fractal sets that we have met in the preceding sections have random analogues. For example, in the von Koch curve construction, each time we replace the middle third of an interval by the other two sides of an equilateral triangle, we might toss a coin to determine whether to position the new part above or below the removed segment. After a few steps, we get a rather irregular-looking curve which, nevertheless, retains certain characteristics of the von Koch curve (Fig. 9).

The middle third Cantor set construction may be randomized in two different ways (Fig. 10). Each time we divide a segment into three parts we could, instead of always removing the middle

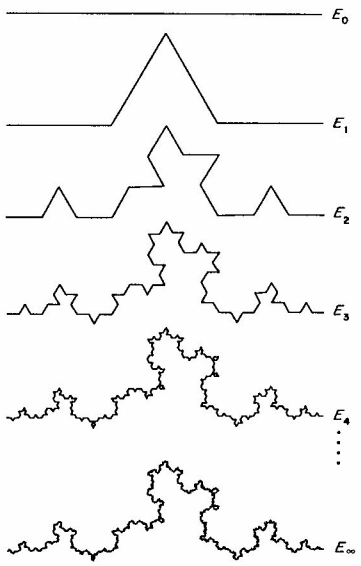

Fig. 9. Random von Koch curve.

segment, throw a die to decide which part to remove. Alternatively, we might choose the interval lengths at each stage of the construction at random, according to a given statistical distribution.

Whilst such random fractals do not have the self-similarity of their non-random counterparts, their non-uniform appearance is often rather closer to natural phenomena such as coastlines, topographical surfaces or fracture surfaces. We could say that the random fractals are *statistically self-similar* in the sense that enlargements of de-

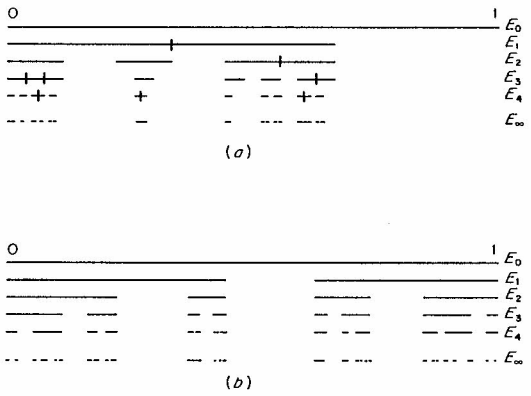

Fig. 10. Random Cantor set.

tails have the same statistical distribution as the whole set.

It is possible to demonstrate a statistical version of Eq. (10), when the factors c_i present a given probability density $p(c_i)$ over the basic interval $[0, c_i^{\max}]$:

$$1 = \sum_{i=1}^{m} \frac{\int_0^{c_i^{\max}} c_i^{\alpha} p(c_i)\, \mathrm{d}c_i}{\int_0^{c_i^{\max}} p(c_i)\, \mathrm{d}c_i}. \tag{22}$$

The two limit cases are represented by "deterministic chaos", with $p(c_i)$ provided by a δ-Dirac function and Eq. (22) reduced to Eq. (10), and by "completely random chaos", with $p(c_i) = 1/c_i^{\max}$.

Regarding the latter situation, let us consider the random von Koch curve, c being a completely random variable with uniform distribution on the interval $[0, \frac{1}{3}]$. At each stage, a segment of length 1 is replaced by four segments of lengths $\frac{1}{2}(1-a)$, a, a, $\frac{1}{2}(1-a)$, respectively, so we have $m = 4$, and $c_1 = c_4 = \frac{1}{2}(1-a)$ and $c_2 = c_3 = a$. Since in this case $p(c_i) = 3$ for $i = 1, 2, 3, 4$, Eq. (22) becomes:

$$1 = \int_0^{1/3} 3 \times 2\left\{\left[\tfrac{1}{2}(1-a)\right]^{\alpha} + a^{\alpha}\right\} \mathrm{d}a, \tag{23}$$

or

$$\alpha + 1 = 12 \times 2^{-(\alpha+1)} - 6 \times 3^{-(\alpha+1)}, \tag{24}$$

so that $\alpha \simeq 1.144$.

5. Fractal nature of material ligament and size effects on nominal tensile strength

It is well-known that the nominal tensile strength of many materials undergoes very clear size effects. The usual trend is that of a strength decreasing with size, and this is more evident for disordered (i.e. macroscopically heterogeneous and/or damaged) materials. Griffith (1921) explained the strength size effect in the case of glass filaments, assuming the existence of inherent microcracks of a size proportional to the filament cross-section diameter. Some years later Weibull (1939) gave a purely statistical explanation to the same phenomenon according to the weakest-link-in-a-chain concept. Only recently the two views have been harmonized, enriching the empirical approach of Weibull with the phenomenological assumption of Griffith (Freudenthal, 1968; Jayatilaka, 1979; Carpinteri, 1989a). A *statistical size distribution of self-similarity* may be defined (Carpinteri, 1986a; 1989a) for which the most dangerous defect proves to be of a size proportional to the structural size. This corresponds to materials presenting a considerable dispersion in the statistical microcrack size distribution (disordered materials). In this case, the power of the LEFM stress singularity, $1/2$, turns out to be the slope of the strength versus size decrease in a bilogarithmic diagram. When the statistical dispersion is relatively low (ordered materials) the slope is less than $1/2$ and tends to zero for regular distributions (perfectly ordered materials).

Although the above-described view contains the fractal concept of self-similarity, this is circumscribed only to the defect of maximum size, whereas the disordered nature of the material microstructure is completely disregarded. The real nature of the material will be herein described through a more complex fractal model, where the property of self-similarity is extended to the whole defect population. This model represents a more realistic picture of reality and is consistent with the fractal explanation to the fracture energy size effect, which will be proposed in the next section. On the other hand, as will be shown, slope values higher than $1/2$ would represent, with both models, a degree of disorder that is so high that it is usually absent in real materials.

Let us assume that the reacting section or ligament of a disordered material at peak stress could be represented as a fractal space of dimension $\alpha = 2 - d_\sigma$, with $1 < \alpha \leqslant 2$ and, therefore, $0 \leqslant d_\sigma < 1$. The dimensionality decrement d_σ may be due to the presence of cracks and voids and then, generally, to a cross-sectional weakening. Let us consider two bodies, geometrically similar and made up of the same disordered material (Fig. 11). If the ratio of geometrical similitude is equal to b and the *fractal tensile strength* σ_u^* is assumed to be a material constant and to have

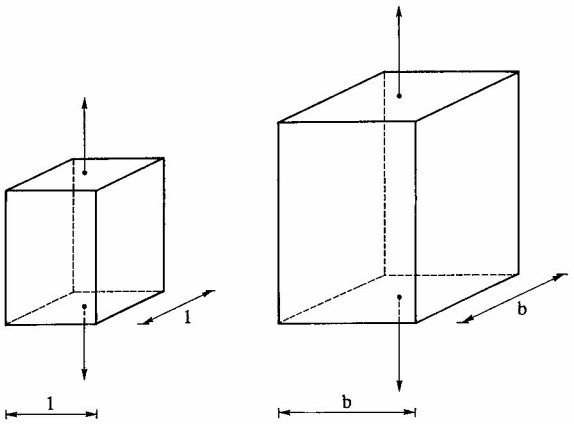

Fig. 11. Geometrically similar bodies where b is the ratio of geometrical similitude.

the physical dimensions [force] $\times$ [length]$^{-(2-d_\sigma)}$, we have:

$$\sigma_u^* = \frac{F_1}{1^{2-d_\sigma}} = \frac{F_2}{b^{2-d_\sigma}}, \tag{25}$$

F_1 and F_2 being the ultimate tensile forces acting on the two bodies, respectively.

On the other hand, the apparent nominal tensile strengths are respectively:

$$\sigma_u^{(1)} = \frac{F_1}{1^2}, \tag{26a}$$

$$\sigma_u^{(2)} = \frac{F_2}{b^2}, \tag{26b}$$

where the latter, according to Eq. (25), becomes:

$$\sigma_u^{(2)} = \sigma_u^{(1)} b^{-d_\sigma}. \tag{27}$$

We can write the relationship between nominal strengths related to different sizes in logarithmic form:

$$\ln \sigma_u = \ln \sigma_u(1) - d_\sigma \ln b. \tag{28}$$

Eq. (28) represents a straight line with slope $-d_\sigma$ in the ln σ_u versus ln b plane (Fig. 12).

Confirmation of Eq. (28) has been provided by several previous investigations, carried out on different metallic or cementitious materials and with different specimen geometries: tension, bending, Brazilian, etc. These results are summarized in Carpinteri (1989a). The same trends have been found also in two recent experimental programs

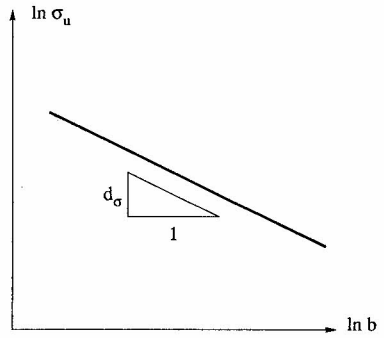

Fig. 12. Nominal tensile strength decrease with specimen size.

aimed at evaluating the true tensile properties of concrete. A completely new testing apparatus made up of three orthogonally disposed actuators, was utilized at the Politecnico di Torino so that it was possible to perform a true direct tensile experiment on concrete (Carpinteri and Maradei, 1994, Carpinteri and Ferro, 1994), whereas usually tension and bending are both present. As may be seen from Fig. 13, the slope of the strength decrease proves to be equal to 0.14, thus revealing a material ligament of dimen-

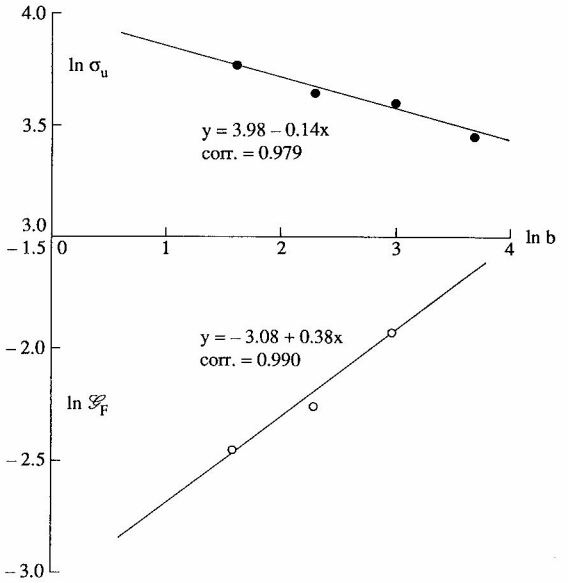

Fig. 13. Variations in tensile strength and fracture energy with specimen size. Tensile tests in (Carpinteri and Maradei, 1994; Carpinteri and Ferro, 1994): σ_u measured in kg/cm^2; $\mathscr{G}_F$ measured in kg/cm; b measured in cm.

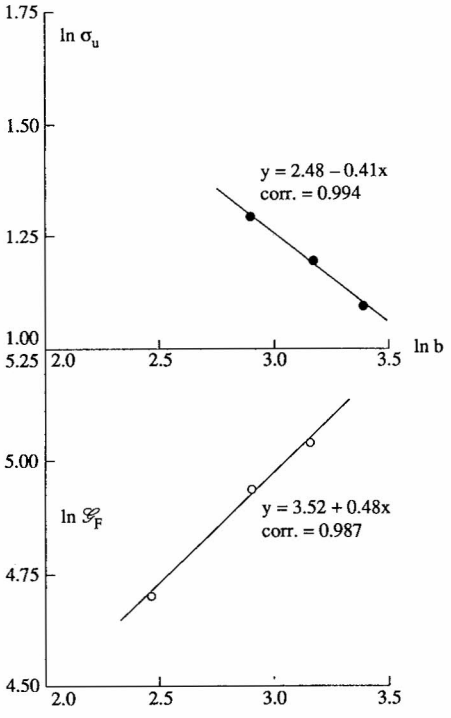

Fig. 14. Variations in tensile strength and fracture energy with specimen diameter. Tensile tests in (Carpinteri et al., 1994): σ_u measured in MPa; $\mathscr{G}_F$ measured in N/m; b measured in cm.

sion 1.86, i.e. a fractal set which is very close to a two-dimensional surface. It may be noted that the specimen sizes explored in this investigation ranged over four values of the width: 5, 10, 20, 40 cm. The fractal nature of the material ligament emerges very clearly at such scales. On the other hand the property of self-similarity is very likely to vanish or change at higher or lower scales, owing to the limited character of the granulometric curve.

Higher slope of the strength decrease is obtained in an experimental research study performed at ISMES–Bergamo (Carpinteri et al., 1994), using pre-notched concrete cylinders of diameter 12, 18, 24, 30 cm, respectively (Fig. 14). The exponent 0.41 is closer to the LEFM limit 0.5, which is valid for disordered materials (high statistical dispersion), and, at the same time, it implies a very weak fractal ligament of dimension 1.59 at peak stress.

6. Fractal nature of fracture surface and size effects on fictitious fracture energy

It is well-known how the fracture surfaces of metals (Mandelbrot et al., 1984) and concrete (Saouma et al., 1990) present a fractal nature with a roughness producing a dimensional increment with respect to the number 2. Even in this case we can detect an evident mechanical consequence, considering the size effects on fracture energy $\mathscr{G}_F$. Since Hillerborg's proposal for a concrete fracture test was published as RILEM Recommendation (1985), several researchers have measured a fracture energy $\mathscr{G}_F$ which increases with the specimen sizes, and, more specifically, with the size of the uncracked ligament. Such a trend has been systematically found and in each case the authors of the papers describing these experiments have tried to provide various empirical or phenomenological explanations, without, however, endeavouring to interpret their findings in a larger conceptual framework. On the other hand, if we wish to understand the experimental observations, it is necessary to abandon the classical thermodynamic concept of surface energy of an ideal solid, and to assume the energy dissipation to be occurring in a fractal space of dimension $\alpha = 2 + d_{\mathscr{G}}$, with $2 \leqslant \alpha < 3$ and, therefore, $0 \leqslant d_{\mathscr{G}} < 1$. This represents an attenuation of fracture localization due to material heterogeneity and multiple cracking.

Let us consider two bodies, geometrically similar and made up of the same disordered material (Fig. 11). If the ratio of geometrical similitude is equal to b and the *fractal fracture energy* $\mathscr{G}_F^*$ is assumed to be a material constant and to have the physical dimensions [force] × [length]$^{-(1+d_{\mathscr{G}})}$, we obtain:

$$\mathscr{G}_F^* = \frac{E_1}{1^{2+d_{\mathscr{G}}}} = \frac{E_2}{b^{2+d_{\mathscr{G}}}}, \tag{29}$$

E_1 and E_2 being the energies dissipated in the two bodies, respectively.

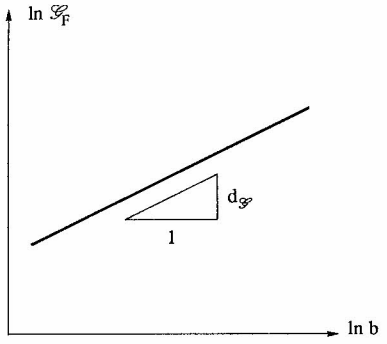

Fig. 15. Fictitious fracture energy increase with specimen size.

On the other hand, the apparent fictitious fracture energies are respectively:

$$\mathcal{G}_F^{(1)} = \frac{E_1}{1^2}, \tag{30a}$$

$$\mathcal{G}_F^{(2)} = \frac{E_2}{b^2}, \tag{30b}$$

where the latter, according to Eq. (29), becomes:

$$\mathcal{G}_F^{(2)} = \mathcal{G}_F^{(1)} b^{d_{\mathcal{G}}}. \tag{31}$$

We can write the relationship between fracture energies related to different sizes in logarithmic form:

$$\ln \mathcal{G}_F = \ln \mathcal{G}_F(1) + d_{\mathcal{G}} \ln b. \tag{32}$$

Eq. (32) represents a straight line with slope $d_{\mathcal{G}}$ in the ln $\mathcal{G}_F$ versus ln b plane (Fig. 15).

The same trends have been found in recent experimental studies. Tensile testing performed at the Politecnico di Torino (Carpinteri and Maradei, 1994; Carpinteri and Ferro, 1994) provides a plot slope equal to 0.38 (Fig. 13), which allows a constant (universal) energy parameter to be obtained in the case where the dissipation is considered as occurring in a damaged space of dimension 2.38. Tensile testing at ISMES–Bergamo (Carpinteri et al., 1994) (Fig. 14) provides a plot slope very close to the LEFM singularity 1/2, namely 0.48, and thus a fractal dimension 2.48, which implies a very disordered material. It is interesting to observe that the range of self-similarity does not extend to the largest size for $\mathcal{G}_F$, just as it does not extend to the smallest size for σ_u. So the ranges of self-similarity for fracture energy and tensile strength do not necessarily coincide.

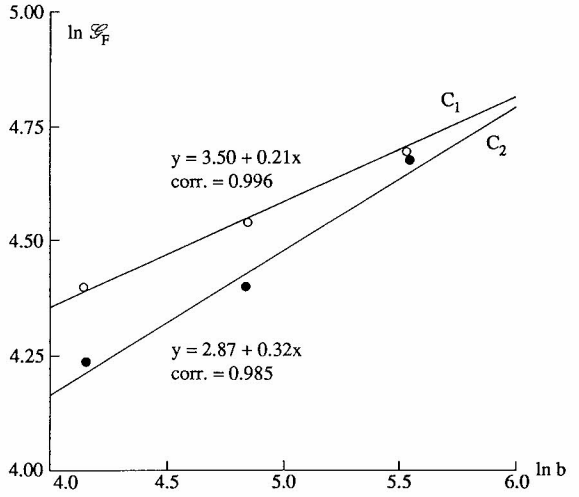

Fig. 16. Variation in fracture energy with beam specimen depth. Bending tests in (Perdikaris and Romeo, 1992): $\mathcal{G}_F$ measured in N/m; b measured in mm.

Even in the paper by Perdikaris and Romeo (1992) the fracture energy evaluated according to RILEM appears as steadily increasing (Fig. 16). The high strength concrete, which is the less tough and is indicated with C_2 in the diagram, presents a slope equal to 0.32, whilst the low

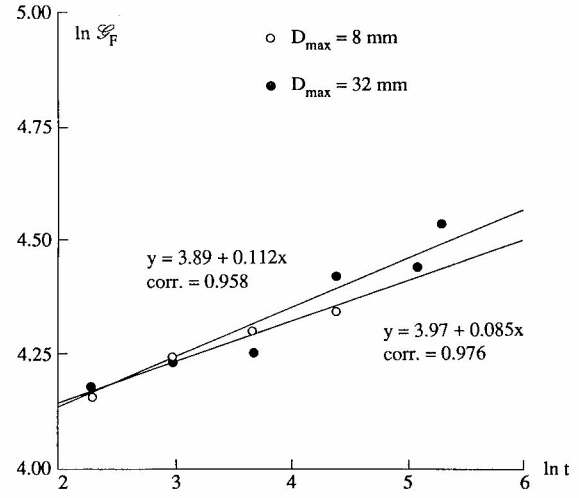

Fig. 17. Variation in fracture energy with specimen thickness. Wedge splitting tests in (Wittmann, 1992): $\mathcal{G}_F$ measured in N/m, t measured in mm.

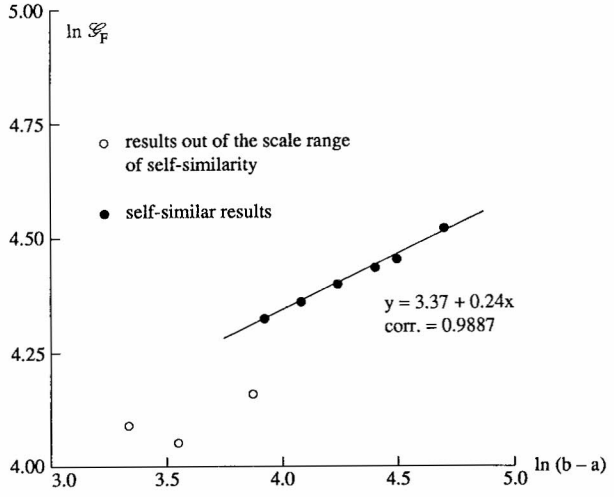

Fig. 18. Variation in fracture energy with specimen ligament. Wedge splitting tests in (Wittmann, 1992): $\mathscr{G}_F$ measured in N/m; $(b-a)$ measured in mm.

strength concrete, which is indicated with C_1 in the diagram, presents a slope equal to 0.21. The three data are related to three-point bending specimens of depth 64, 128, 256 mm, respectively.

A very recent confirmation of fracture energy increase with size was given by Wittmann (1992), using the wedge-splitting technique with concrete slices of thickness varying between 10 and 200 mm (Fig. 17). In the case of maximum aggregate size $D_{max} = 8$ mm the slope is very weak, 0.085, whereas for $D_{max} = 32$ mm the slope becomes 0.112 (more disordered material). In any case the slope appears considerably smaller for a thickness effect than for a width effect.

A second investigation by Wittmann (1992) was devoted to the ligament effect (ligament = $(b-a)$; b = specimen width; a = initial crack length). With specimens of width 150 or 200 mm, the ligament effect is described in Fig. 18, the ligament ranging from 28 to 110 mm. It is found that only from 50 mm upwards is the self-similarity respected, the three results related to 28, 35 and 48 mm, respectively, being non-aligned with the others. This is consistent with the relatively large aggregate size of 32 mm. The correlation coefficient proves very high for the data between 50 and 110 mm, namely 0.9887. The slope of the regression line is equal to 0.24.

7. Conclusions

The abundant literature on tensile strength and fracture energy size effects as well as the newly-introduced fractal theories would appear to indicate the need for a dramatic change in the conceptual framework and even in our whole way of thinking, if we want to consider and measure material constants in strength of materials as well as in fracture mechanics. This means that we have to give up ideal reference areas when we consider the tensile strength and fracture energy of disordered materials with a fractal microstructure. The socalled homogeneous materials (on the macroscopic scale or macrolevel) present, on the other hand, a very small deviation from the ideal case. Only on the microscopic scale or microlevel might they present a higher degree of fractality (Meakin, 1991). For concrete and rocks, for which the micro- and mesolevel coincide with the structural level, the tensile strength is given by a force acting on a surface having a fractal dimension lower than 2, while the fracture energy is represented by a dissipation over a surface with a fractal dimension higher than 2.

In the case of tensile strength the dimensional decrement represents self-similar weakening of the reacting cross section or ligament, due to pores, voids, defects, cracks, aggregates, inclusions, etc. Likewise, in the case of fracture energy, the dimensional increment represents self-similar tortuosity of the fracture surface, due to aggregates and inclusions, as well as self-similar microcrack overlapping and distribution even in the direction orthogonal to that of the forming macrocrack (Fig. 7) (van Mier, 1992). It is possible to prove that, when the ratio of the generic microcrack to the immediately larger hierarchical microcrack is larger than $\sqrt{2}/2$, energy dissipation occurs in the volume instead of on a fractal surface, see Eq. (16):

$$1 = 2(x)^2, \quad \text{or} \quad x = \sqrt{2}/2. \tag{33}$$

Regarding the dimensional decrement d_σ and the dimensional increment $d_{\mathscr{G}}$, experimentally they appear always comprised in the interval $[0, \frac{1}{2}]$. The dimensional decrement d_σ tends to the LEFM limit $\frac{1}{2}$ only for extremely brittle and

disordered materials (defect size distribution of self-similarity) and is connected to the Weibull parameter m in the case of planar similitude (Carpinteri, 1989a):

$$d_\sigma = 2/m. \tag{34}$$

Even the dimensional increment $d_{\mathscr{G}}$ tends to the same limit $\frac{1}{2}$ for extremely brittle and disordered materials. The explanation for the latter bound could arise for dimensional analysis reasons. A generalization of the *brittleness number* defined by the writer (Carpinteri, 1981a; 1981b; 1982, 1985, 1986b, 1989b) could in fact be the following:

$$s_E^* = \frac{\mathscr{G}_F^*}{\sigma_u^* b^{(1-d_\sigma-d_{\mathscr{G}})}}. \tag{35}$$

If we postulate that the reversal of the physical roles of toughness and strength is absurd, the exponent of the characteristic linear size b must be positive:

$$d_\sigma + d_{\mathscr{G}} < 1. \tag{36}$$

The sum of the dimensional decrement (for material ligament) and the dimensional increment (for fracture surface) must therefore be lower than unity. On the other hand, when, for very disordered materials, we have $d_\sigma \simeq \frac{1}{2}$, the upper bound of Eq. (36) becomes: $d_{\mathscr{G}} \lesssim \frac{1}{2}$.

The above fractal interpretations could be regarded by some as purely mathematical abstractions, if not indeed distortions of reality. The truth is that both classical geometrical domains and fractal geometrical loci are idealizations of reality. The question that should be answered is the following: which model is closer to a real fracture trajectory in a concrete specimen: a straight line or the von Koch curve? Of course the latter, even though the fractal nature of the fracture trajectory is random and valid only in a limited scale range. This means that, for size scales tending to infinity, or, in other words, for very large specimens, tensile strength σ_u and fracture energy $\mathscr{G}_F$ may appear constant by varying the specimen size, whereas, for size scales where random self-similarity holds, the so-called "universal properties" of the system $(\sigma_u^*, \mathscr{G}_F^*)$ are constant, although they are represented by physical quantities with unusual dimensions. The last result represents the target of the so-called "renormalization" procedure (Wilson, 1971), i.e. the determination of physical quantities that are invariant under a change of length scale.

Acknowledgements

The present research was carried out with the financial support of the Ministry of University and Scientific Research (MURST) and the National Research Council (CNR).

References

Carpinteri, A. (1981a), Experimental determination of fracture toughness parameters K_{IC} and J_{IC} for aggregative materials, Proc. Fifth Int. Conf. on Fracture, Pergamon Press, Oxford, pp. 1491–1498.

Carpinteri, A. (1981b), Static and energetic fracture parameters for rocks and concretes, *Mater. Struct. 14*, 151–162.

Carpinteri, A. (1982), Notch sensitivity in fracture testing of aggregative materials, Eng. Fract. Mech. 16, 467–481.

Carpinteri, A. (1983), Plastic flow collapse vs. separation collapse (fracture) in elastic–plastic strain-hardening structures, *Mater. Struct. 16*, 85–96.

Carpinteri, A. and A.R. Ingraffea, eds. (1984), *Fracture Mechanics of Concrete: Material Characterization and Testing*, Martinus Nijhoff Publishers, The Hague.

Carpinteri, A. (1985), Interpretation of the Griffith instability as a bifurcation of the global equilibrium, in: S.P. Shah, ed., *Applications of Fracture Mechanics to Cementitious Composites*, Martinus Nijhoff Publishers, Dordrecht, pp. 287–316.

Carpinteri, A. (1986a), *Mechanical Damage and Crack Growth in Concrete: Plastic Collapse to Brittle Fracture*, Martinus Nijhoff Publishers, Dordrecht.

Carpinteri, A. (1986b), Limit analysis for elastic-softening structures: scale and slenderness influence on the global brittleness, in: A.M. Brandt and I.H. Marshall, eds., *Brittle Matrix Composites*, Elsevier Applied Science, London and New York, pp. 497–508.

Carpinteri, A. (1987), Stress-singularity and generalized fracture toughness at the vertex of re-entrant corners, *Eng. Fract. Mech. 26*, 143–155.

Carpinteri, A. (1989a), Decrease of apparent tensile and bending strength with specimen size: two different explanations based on fracture mechanics, *Int. J. Solids Struct. 25*, 407–429.

Carpinteri, A. (1989b), Cusp catastrophe interpretation of fracture instability, *J. Mech. Phys. Solids 37*, 567–582.

Carpinteri, A., ed. (1992), *Applications of Fracture Mechanics to Reinforced Concrete*, Elsevier Applied Science, London and New York.

Carpinteri, A. and F. Maradei (1994), Experimental mechanics, to appear.

Carpinteri, A. and G. Ferro (1994), Materials and structures, to appear.

Carpinteri, A., G. Ferrara and L. Imperato (1994), Engineering fracture mechanics, to appear.

Elices, M., G.V. Guinea and J. Planas (1992), Measurement of the fracture energy using three-point bend tests; Part 3 – Influence of cutting the $P-\delta$ tail, *Mater. Struct. 25*, 327–334.

Falconer, K. (1990), *Fractal Geometry: Mathematical Foundations and Applications*, John Wiley & Sons, Chichester.

Freudenthal, A.M. (1968), Statistical approach to brittle fracture, in: H. Liebowitz, ed., *Fracture*, Vol. 2, Academic Press, New York, pp. 591–619.

Griffith, A.A. (1921), The phenomena of rupture and flow in solids, *Philos. Trans. R. Soc. London A221*, 163–198.

Guinea, G.V., J. Planas and M. Elices (1992), Measurement of the fracture energy using three-point bend tests: Part 1 – Influence of experimental procedures, *Mater. Struct. 25*, 212–218.

Herrmann, H.J. and S. Roux, eds. (1990), *Statistical Models for the Fracture of Disordered Media*, North-Holland, Amsterdam.

Hu, X.Z. and F.H. Wittmann (1992), Fracture energy and fracture process zone, *Mater. Struct. 25*, 319–326.

Irwin, G.R. (1957), Analysis of stresses and strains near the end of a crack traversing a plate, *J. Appl. Mech. 24*, 361–364.

Jayatilaka, A.S. (1979), *Fracture of Engineering Brittle Materials*, Applied Science, London.

Long, Q.Y., L.I. Suqin and C.V. Lung (1991), Studies on the fractal dimension of a fracture surface formed by slow stable crack propagation, *J. Appl. Phys. 24*, 602–607.

Mackin, T.J., J.J. Mecholsky Jr., D.E. Passoja and Y.L. Tsai (1990), Scaling concepts applied to brittle fracture, *Proc. Symp. W, 1990 Fall Meeting of the Materials Research Society*, Boston, pp. 33–36.

Mandelbrot, B.B. (1982), *The Fractal Geometry of Nature*, W.H. Freemann and Company, New York.

Mandelbrot, B.B., D.E. Passoja and A.J. Paullay (1984), Fractal character of fracture surfaces of metals, *Nature 308*, 721–722.

Mazars, J. and Z.P. Bažant, eds. (1989), *Cracking and Damage: Strain Localization and Size Effect*, Elsevier Applied Science, London and New York.

Meakin, P. (1991), Models for material failure and deformation, *Science 252*, 226–234.

Panagiotopoulos, P.D. (1992), Fractal geometry in solids and structures, *Int. J. Solids Struct. 29*, 2159–2175.

Perdikaris, P.C. and A. Romeo (1992), Effect of size and compressive strength on the fracture energy of plain concrete, *Proc. First Int. Conf. on Fracture Mechanics of Concrete Structures* (FraMCoS1), Elsevier Applied Science, London and New York, pp. 550–555.

Planas, J., M. Elices and G.V. Guinea (1992), Measurement of the fracture energy using three-point bend tests: Part 2 – Influence of bulk energy dissipation, *Mater. Struct. 25* 305–312.

RILEM Technical Committee 50 (1985), Determination of the fracture energy of mortar and concrete by means of three-point bend tests on notched beams, Draft Recommendation, *Mater. Struct. 18*, 287–290.

Saouma, V.E., C.C. Barton and N.A. Gamaleldin (1990), Fractal characterization of fracture surfaces in concrete, *Eng. Fract. Mech. 35*, 47–53.

Shah, S.P. and A. Carpinteri, eds. (1991), *Fracture Mechanics Test Methods for Concrete*, Chapman & Hall, London.

van Mier, J.G.M. (1992), Scaling in tensile and compressive fracture of concrete, in: A. Carpinteri, ed., *Applications of Fracture Mechanics to Reinforced Concrete*, Elsevier Applied Science, London and New York, pp. 95–135.

van Mier, J.G.M., J.G. Rots and A. Bakker, eds. (1991), *Fracture Processes in Concrete, Rock and Ceramics*, Chapman & Hall, London.

Weibull, W. (1939), *A Statistical Theory of the Strength of Materials*, Swedish Royal Institute for Engineering Research, Stockholm.

Wilson, K.G. (1971), Renormalization group and critical phenomena, *Phys. Rev. B4*, 3174–3205.

Wittmann, F.H. (1992), Fracture process zone and fracture energy, *Proc. First Int. Conf. on Fracture Mechanics of Concrete Structures* (FraMCoS1) Elsevier Applied Science, London and New York, pp. 391–403.